
Research Article: New Research | Neuronal Excitability

Excitatory Neuronal Responses of Ca²⁺ Transients in Interstitial Cells of Cajal in the Small Intestine

Salah A. Baker¹, Bernard T. Drumm¹, Karolina E Skowronek¹, Benjamin E. Rembetski¹, Lauren E Peri¹, Grant W. Hennig², Brian A Perrino¹ and Kenton M. Sanders¹

¹Department of Physiology and Cell Biology, University of Nevada School of Medicine, Reno, NV 89557, USA

²Department of Pharmacology, University of Vermont, Burlington, VT 05405, USA

DOI: 10.1523/ENEURO.0080-18.2018

Received: 21 February 2018

Accepted: 12 March 2018

Published: 16 March 2018

Author contributions: S.A.B., B.T.D., and K.M.S. designed research; S.A.B., B.T.D., K.E.S., B.E.R., L.P., G.W.H., B.A.P., and K.M.S. performed research; S.A.B., B.T.D., and K.M.S. contributed unpublished reagents/analytic tools; S.A.B., B.T.D., K.E.S., B.E.R., L.P., G.W.H., B.A.P., and K.M.S. analyzed data; S.A.B., B.T.D., and K.M.S. wrote the paper.

Funding: <http://doi.org/10.13039/100000062HHS> | NIH | National Institute of Diabetes and Digestive and Kidney Diseases (NIDDK) P01 DK41315 P30-GM110767

The authors declare no competing financial interests.

HHS | NIH | National Institute of Diabetes and Digestive and Kidney Diseases (NIDDK) [P01 DK41315] [P30-GM110767].

S.A.B. and B.T. Drumm contributed equally to this work.

Corresponding author: Kenton M. Sanders, Department of Physiology and Cell Biology, University of Nevada School of Medicine, MS 352, Reno, NV, 89557, USA. Phone: (775) 784-6061. Fax (775) 784-6903. E-mail: ksanders@medicine.Nevada.edu

Cite as: eNeuro 2018; 10.1523/ENEURO.0080-18.2018

Alerts: Sign up at eneuro.org/alerts to receive customized email alerts when the fully formatted version of this article is published.

Accepted manuscripts are peer-reviewed but have not been through the copyediting, formatting, or proofreading process.

Copyright © 2018 Baker et al.

This is an open-access article distributed under the terms of the Creative Commons Attribution 4.0 International license, which permits unrestricted use, distribution and reproduction in any medium provided that the original work is properly attributed.

1 **Excitatory neuronal responses of Ca²⁺ transients in interstitial**
2 **cells of Cajal in the small intestine**

3 *Salah A. Baker¹, *Bernard T. Drumm¹, Karolina E Skowronek¹, Benjamin E.
4 Rembetski¹, Lauren E Peri¹, Grant W. Hennig², Brian A Perrino¹ & Kenton M.
5 Sanders¹.

6 1 *Department of Physiology and Cell Biology,*
7 *University of Nevada School of Medicine,*
8 *Reno, NV 89557, USA*

9 2 *Department of Pharmacology,*
10 *University of Vermont, Burlington,*
11 *VT 05405, USA.*

12
13 **Abbreviated title:** Regulation of Ca²⁺ transients in ICC by excitatory neurons

14 **Corresponding author:** Kenton M. Sanders, Department of Physiology and Cell
15 Biology, University of Nevada School of Medicine, MS 352, Reno, NV, 89557,
16 USA. Phone: (775) 784-6061. Fax (775) 784-6903.

17 E-mail: ksanders@medicine.nevada.edu¹

18 **Number of pages:** 48

19 **Number of figures:** 13; **Number of tables** 1; **Number of multimedia** 1

20 **Number of words:** Abstract 218; Introduction 774; Discussion 1422

21 **Conflict of interest:** None. The authors declare no competing financial interests

22 **Acknowledgements:** The authors are grateful to Ms. Nancy Horowitz for help
23 with breeding of animals and tamoxifen treatments. ICC were purified by FACS

*Salah A. Baker and Bernard T. Drumm contributed equally to this work

24 from enzymatic dispersions of jejunal muscles in the Cell Cytometry and FACS
25 Core Laboratory supported by a Phase III COBRE award from the NIGMS (P30-
26 GM110767). This Core was developed and supervised by the late Dr. Douglas
27 Redelman and more recently by Mr. Byoung Koh. This project was funded by
28 P01 DK41315 from the NIDDK.

29

30

31

32

33

34

35

36

37

38

39

40

41

42

43

44

45

46

47 **Abstract**

48

49 Interstitial cells of Cajal (ICC) regulate smooth muscle excitability and motility in
50 the gastrointestinal tract. ICC in the deep muscular plexus (ICC-DMP) of the
51 small intestine are aligned closely with varicosities of enteric motor neurons and
52 thought to transduce neural responses. ICC-DMP generate Ca^{2+} transients that
53 activate Ca^{2+} activated Cl^- channels and generate electrophysiological responses.
54 We tested the hypothesis that excitatory neurotransmitters regulate Ca^{2+}
55 transients in ICC-DMP as a means of regulating intestinal muscles. High-
56 resolution confocal microscopy was used to image Ca^{2+} transients in ICC-DMP
57 within murine small intestinal muscles with cell-specific expression of GCaMP3.
58 Intrinsic nerves were stimulated by electrical field stimulation (EFS). ICC-DMP
59 exhibited ongoing Ca^{2+} transients before stimuli were applied. EFS caused initial
60 suppression of Ca^{2+} transients, followed by escape during sustained stimulation,
61 and large increases in Ca^{2+} transients after cessation of stimulation. Basal Ca^{2+}
62 activity and the excitatory phases of Ca^{2+} responses to EFS were inhibited by
63 atropine and neurokinin 1 receptor (NK1) antagonists, but not by NK2 receptor
64 antagonists. Exogenous ACh and substance P increased Ca^{2+} transients,
65 atropine and NK1 antagonists decreased Ca^{2+} transients. Neurokinins appear to
66 be released spontaneously (tonic excitation) in small intestinal muscles and are
67 the dominant excitatory neurotransmitters. Subcellular regulation of Ca^{2+} release
68 events in ICC-DMP may be a means by which excitatory neurotransmission
69 organizes intestinal motility patterns.

70 **Significance statement:**

71 Interstitial cells of Cajal (ICC) are innervated by enteric motor neurons and
72 thought to transduce neural responses in GI muscles.

73 Ca^{2+} transients, due to Ca^{2+} release from Ca^{2+} intracellular stores, mediate
74 electrophysiological events in ICC by activation of Ca^{2+} -activated Cl^- channels.

75 Neural responses in ICC in the deep muscular plexus of the small intestine (ICC-
76 DMP) were studied by confocal imaging of Ca^{2+} transients in these cells.

77 Excitatory neural input was due to cholinergic and peptidergic neurotransmitters
78 (acetylcholine and neurokinins), as excitatory effects on Ca^{2+} transients were
79 blocked by atropine and neurokinin receptor antagonists. Neurokinins are the
80 dominant excitatory regulators of Ca^{2+} transients in ICC-DMP. ICC-DMP are
81 innervated by enteric motor neurons and mediate significant excitatory responses
82 in intestinal muscles.

83

84

85

86

87

88

89

90

91

92

93 **Introduction**

94 Muscles of the gastrointestinal (GI) tract are innervated by both excitatory
95 and inhibitory enteric motor neurons (Furness, 2012), and motility patterns of the
96 gut depend upon the outputs of the enteric nervous system. Neural inputs are
97 overlaid upon the basal excitability of the smooth muscle cells (SMCs) that line
98 the walls of GI organs. SMC excitability is determined by ionic conductances and
99 Ca^{2+} sensitization mechanisms intrinsic to these cells but also by interstitial cells
100 that are electrically coupled to SMCs. Together SMCs and interstitial cells (i.e.
101 interstitial cells of Cajal (ICC) and platelet derived growth factor receptor α -
102 immunopositive (PDGFR α^+) cells (Komuro, 2006; Sanders and Ward, 2006; Iino
103 et al., 2009; Blair et al., 2012; Baker et al., 2013) form an electrical syncytium,
104 known as the SIP syncytium (Sanders et al., 2012). It is the integrated output of
105 these cells that determines the basal excitability of GI smooth muscle tissues and
106 ultimately the responses to enteric motor neurons and other higher order
107 regulatory pathways (Sanders et al., 2014a).

108 In the small intestine, a network of ICC in the myenteric region (ICC-MY)
109 serves as the pacemaker cells that generate and actively propagate electrical
110 slow waves and organize contractile activity into a phasic pattern that underlies
111 segmental contractions (Langton et al., 1989; Ward et al., 1994; Ordog et al.,
112 1999; Sanders et al., 2014a). Another class of ICC are distributed within smooth
113 muscle bundles in the deep muscular plexus (ICC-DMP; (Rumessen et al., 1992;
114 Zhou and Komuro, 1992)) throughout the smooth muscle organs of the GI tract.
115 ICC-DMP are innervated by motor neurons and transduce part of the input from

116 enteric motor neurons (Wang et al., 2003b; Iino et al., 2004; Ward et al., 2006).
117 This conclusion is based on the fact that ICC-DMP are: i) closely apposed to
118 varicosities of enteric motor neurons, forming synaptic-like contacts (i.e. <20 nM;
119 (Rumessen et al., 1992; Zhou and Komuro, 1992); ii) express major receptors for
120 enteric motor neurotransmitters (Sternini et al., 1995; Vannucchi et al., 1997;
121 Chen et al., 2007); and iii) display evidence of receptor binding, receptor
122 internalization, and translocation of signaling molecules upon nerve stimulation
123 (Wang et al., 2003b; Iino et al., 2004). iv) electrically coupled to SMCs via gap
124 junctions (Daniel et al., 1998; Daniel and Wang, 1999; Seki and Komuro, 2001).
125 Experiments in other regions of the GI tract, where ICC-IM are lost in mutant
126 animals have shown distinct changes in motor neurotransmission in the absence
127 of ICC (Daniel and Posey-Daniel, 1984; Burns et al., 1996; Komuro et al., 1999;
128 Ward et al., 2000; Klein et al., 2013). Nevertheless, there is controversy about
129 the importance of ICC in neurotransmission, and some investigators have argued
130 that ICC are not important elements in enteric nerve responses (Goyal and
131 Chaudhury, 2010; Goyal, 2016).

132 A fundamental mechanism involved in the activation of ICC (as
133 pacemakers and in regulating the excitability of GI muscles) is Ca^{2+} release from
134 intracellular stores (van Helden and Imitiaz, 2003; Lee et al., 2007; Baker et al.,
135 2016; Drumm et al., 2017). Ca^{2+} release is important because it activates Ca^{2+} -
136 activated Cl^- channels (CaCC), encoded by *Ano1*, that are strongly expressed in
137 ICC (Chen et al., 2007; Gomez-Pinilla et al., 2009; Zhu et al., 2015). We have
138 used mice expressing Ca^{2+} sensors specifically in ICC to investigate the Ca^{2+}

139 transients generated by ICC in intact intestinal muscles (Baker et al., 2016;
140 Drumm et al., 2017).

141 Excitatory transmission in the gut is mediated predominantly via
142 cholinergic and neurokinins. Tachykinin (TKs) family of peptides (substance P
143 (SP), neurokinin A (NKA) and B (NKB) are expressed throughout the
144 gastrointestinal tract (Holzer and Holzer-Petsche, 2001; Cipriani et al., 2011;
145 Mitsui, 2011; Steinhoff et al., 2014). SP, NKA and NKB are preferentially
146 mediated through the stimulation of NK1, NK2 and NK3 G-protein-coupled
147 receptors. Both NK1 and NK2 receptors mediate contractile effects in the
148 gut. small intestine, smooth muscle electrical and motor events induced by
149 electrical field stimulation (EFS) can involve either or both NK1 and NK2
150 receptors. But functional evidence support the involvement of NK1 subtype in
151 mediating NANC contractions to EFS in the mouse small intestine (Iino et al.,
152 2004; De Schepper et al., 2005).

153 In the present study we investigated the hypothesis that a major
154 mechanism by which enteric motor neurotransmitters regulate ICC is through
155 modulation of Ca^{2+} release events. To test this hypothesis, we explored whether
156 excitatory neural inputs to ICC-DMP are coupled to Ca^{2+} release and
157 characterized the nature of the Ca^{2+} responses that constitute this transduction
158 pathway for post-junctional excitatory transmission.

159

160 **Methods**

161

162 **Animals**

163 GCaMP3-floxed mice (B6.129S-*Gt(ROSA)26Sor^{tm38(CAG-GCaMP3)Hze}/J*) and
164 their wild-type siblings (C57BL/6) were acquired from Jackson Laboratories (Bar
165 Harbor, MN, USA) and crossed with Kit-Cre mice (*c-Kit^{+Cre-ERT2}*), provided by Dr.
166 Dieter Saur (Technical University Munich, Munich, Germany). Kit-Cre-GCaMP3
167 mice (both sexes) were injected with tamoxifen at 6-8 weeks of age (2 mg for
168 three consecutive days), as previously described (Baker et al., 2016) to activate
169 Cre recombinase and GCaMP3 expression. 15 days after tamoxifen injection,
170 Kit-Cre-GCaMP3 mice were anaesthetized by isoflurane inhalation (Baxter,
171 Deerfield, IL, USA) and killed by cervical dislocation. All animals used for these
172 experiments were handled in compliance with the National Institutes of Health
173 Guide for the Care and Use of Laboratory Animals, and the protocols were
174 approved by the Institutional Animal Use and Care Committee at the University of
175 Nevada, Reno.

176

177 **Tissue preparation**

178 Segments of jejunum (2 cm in length) were removed from mice and
179 bathed in Krebs-Ringer bicarbonate solution (KRB). Jejunal segments were
180 opened along the mesenteric border and luminal contents were washed away
181 with KRB. The mucosa and sub-mucosa layers were removed by sharp

182 dissection, and the remaining *tunica muscularis* was pinned flat within a Sylgard
183 coated dish.

184 **Drugs and Solutions**

185 Tissues were maintained and perfused with KRB containing (mmol/L):
186 NaCl, 120.35; KCl, 5.9; NaHCO₃, 15.5; NaH₂PO₄, 1.2; MgCl₂, 1.2; CaCl₂, 2.5;
187 and glucose, 11.5. The KRB was bubbled with a mixture of 97% O₂ – 3 %CO₂
188 and warmed to 37 ± 0.2 °C.

189 All drugs were purchased from Tocris Bioscience (Ellisville, Missouri,
190 USA) and dissolved in the solvents recommended by the manufacturer to obtain
191 stock solutions. Final concentrations used in experiments were obtained by
192 dilution into KRB.

193

194 **Fluorescence Activated Cell Sorting (FACS), RNA extraction and** 195 **quantitative PCR**

196 Jejunal ICC were dispersed from Kit^{+/copGFP} mice as previously described
197 (Zhu et al., 2009; Zhu et al., 2011). ICC were sorted and purified by FACS
198 (FACSAria II; Becton-Dickinson) using an excitation laser (488 nm) and emission
199 filter (530/30 nm). Sorting was performed using a 130-µm nozzle and a sheath
200 pressure of 12 psi.

201 RNA was prepared from sorted ICC and dispersed jejunal cells of the
202 *tunica muscularis* before sorting using an illustra RNAspin Mini RNA Isolation Kit
203 (GE Healthcare). The PCR primers used and their GenBank accession numbers
204 are provided in Table 1. Quantitative PCR (qPCR) was performed using SYBR

205 green chemistry on the 7500 HT Real-time PCR System (Applied Biosystems)
206 and analyzed, as previously described (Baker et al., 2016). All data sets were
207 normalized to the housekeeping gene *Gapdh*.

208

209 **Calcium imaging**

210 Jejunal muscle sheets (5.0 x 10.0 mm) were pinned to the base of a 5ml,
211 60 mm diameter Sylgard-coated dish. The muscles were perfused with warmed
212 KRB solution at 37°C for an equilibration period of 1 hour. Fluorescence imaging
213 was performed with a spinning-disk confocal microscope (CSU-W1 spinning disk;
214 Yokogawa Electric Corporation) mounted to an upright Nikon Eclipse FN1
215 microscope equipped with a 60x 1.0 NA CFI Fluor lens (Nikon instruments INC,
216 NY, USA). GCaMP3, expressed solely in ICC, was excited at 488 nm using a
217 laser coupled to a Borealis system (ANDOR Technology, Belfast, UK). Emitted
218 fluorescence (>515 nm) was captured using a high-speed EMCCD Camera
219 (Andor iXon Ultra; ANDOR Technology, Belfast, UK). Image sequences were
220 collected at 33 fps using MetaMorph software (Molecular Devices INC, CA, USA).
221 Additional Ca²⁺ imaging data was acquired with an Eclipse E600FN microscope
222 (Nikon Inc., Melville, NY, USA) equipped with a 60x 1.0 CFI Fluor lens (Nikon
223 instruments INC, NY, USA). In this system, GCaMP3 was excited at 488 nm
224 (T.I.L.L. Polychrome IV, Grafelfing, Germany), as previously described (Baker et
225 al., 2013). All Ca²⁺ imaging experiments were performed in the presence of
226 nifedipine (100 nM) to minimize contractile movements.

227

228

229 **Calcium event analysis**

230 Analysis of Ca^{2+} activity in ICC-DMP was performed, as described
231 previously (Baker et al., 2016). Briefly, movies of Ca^{2+} activity in ICC-DMP were
232 converted to a stack of TIFF (tagged image file format) images and imported into
233 custom software (Volumetry G8c, GW Hennig) for analysis. Tissue movement
234 was stabilized to ensure accurate measurement of Ca^{2+} transients from ICC-
235 DMP. Whole cell ROIs were used to generate spatio-temporal (ST) maps of Ca^{2+}
236 activity in individual ICC-DMP. ST maps were then imported as TIFF files into
237 Image J (version 1.40, National Institutes of Health, MD, USA,
238 <http://rsbweb.nih.gov/ij>) for post hoc quantification analysis of Ca^{2+} events.

239

240 **Experimental design and statistical analysis**

241 Ca^{2+} event frequency in ICC-DMP was expressed as the number of
242 events fired per cell per second (sec^{-1}). Ca^{2+} event amplitude was expressed as
243 $\Delta F/F_0$, the duration of Ca^{2+} events was expressed as full duration at half
244 maximum amplitude (FDHM), and Ca^{2+} event spatial spread was expressed as
245 μm of cell propagated per Ca^{2+} event. Unless otherwise stated, data is
246 represented as mean \pm standard error (S.E.M.). Statistical analysis was
247 performed using either a student's *t*-test or with an ANOVA with a Dunnett post
248 hoc test where appropriate. In all statistical analyses, $P < 0.05$ was taken as
249 significant. P values < 0.05 are represented by a single asterisk (*), P values
250 < 0.01 are represented by two asterisks (**), and P values < 0.001 are represented

251 by three asterisks (***) . When describing data throughout the text, n refers to the
252 number of animals used in that dataset while c refers to the numbers of cells
253 used in that same data set.

254

255

256

257 **Results**258 ***Post-junctional modulation of Ca²⁺ signaling in ICC-DMP by enteric nerve***
259 ***stimulation***

260 ICC-DMP displayed intracellular Ca²⁺ transients that fired in a stochastic
261 manner (Figure 1), as reported previously (Baker et al., 2016). Ca²⁺ transients
262 were generated at multiple sites along the length of individual ICC-DMP and
263 were typically localized, demonstrating no mechanism for active or regenerative
264 propagation of these events within individual cells or between cells and no
265 extrinsic mechanism of entrainment, as has been previously suggested (Huizinga
266 et al., 2014). Ca²⁺ transients in ICC-DMP exhibit a range of frequencies,
267 amplitudes, durations and spatial spread (Baker et al., 2016). ICC are thought to
268 be intermediaries in enteric neurotransmission, relaying signals from enteric
269 neurons to smooth muscle cells, that are electrically coupled to ICC (Daniel et al.,
270 1998; Daniel and Wang, 1999). Therefore, we investigated how Ca²⁺ transients
271 are modulated by enteric neurons activated by electric field stimulation (EFS).

272 EFS (10 Hz, 0.5ms for 5 sec trains) caused two distinct Ca²⁺ responses: i)
273 an initial inhibitory phase; ii) an excitatory response that occurred largely after
274 cessation of EFS (movie 1). The initial inhibitory response at the onset of EFS
275 lasted about ~ 2 sec. During this phase Ca²⁺ transients in ICC-DMP ceased
276 (Figure 1 A-C). In the final 3 sec of EFS Ca²⁺ transients escaped from inhibition
277 leading to an excitatory response that persisted into the period after cessation of
278 the stimulus (Figure 1 A). These effects are illustrated by an ST map and Ca²⁺
279 activity traces in Figure 1 B&C. This example demonstrates that in the final 3 sec

280 of EFS and particularly in the 5 sec after cessation of EFS, Ca^{2+} transients were
281 increased relative to the control period, and firing sites within ICC-DMP increased
282 their firing frequency. We also found that the initiation sites for Ca^{2+} transients
283 varied temporally in response to EFS (Figure 1B). These responses were
284 mediated by neuronal inputs, as they were blocked by tetrodotoxin (TTX, 1 μM ,
285 data not shown). As above, after the onset of EFS, an inhibitory response phase
286 occurred, but in subsequent experiments we concentrated on the excitatory
287 aspects of the neural responses.

288 The excitatory Ca^{2+} response to EFS was quantified during the final 3 sec
289 of EFS (Figure 2 A, blue dashed box) and in the 5 sec immediately following EFS
290 (Post EFS, Figure 2 A, green dashed box). In the pre EFS period, the control
291 frequency of Ca^{2+} transients was 1.04 ± 0.08 events sec^{-1} , and this was
292 increased significantly during the final 3 sec period of EFS to 1.8 ± 0.15 events
293 sec^{-1} (Figure 2 B, $P < 0.0001$, $n=23$, $c=56$). The frequency of Ca^{2+} transients in the
294 post EFS period was also significantly increased from control, firing on average
295 at 2.1 ± 0.1 events sec^{-1} (Figure 2 B, $P < 0.0001$, $n=23$, $c=56$). There was a
296 significant increase in Ca^{2+} transient amplitude in the final 3 sec of EFS from 0.8
297 ± 0.06 to 1.1 ± 0.05 $\Delta\text{F}/\text{F}_0$ (Figure 2 C, $P < 0.05$, $n=23$, $c=56$), although there was
298 no significant increase in amplitude in the post EFS period compared to control
299 (Figure 2 C, $P > 0.05$, $n=23$, $c=56$). Ca^{2+} transient duration increased in the final 3
300 sec of EFS from 193 ± 3.7 to 219.6 ± 7.9 ms (Figure 2 D, $P < 0.01$, $n=23$, $c=56$)
301 and was also significantly increased in the post EFS period, increasing to $222 \pm$
302 6.5 ms (Figure 2 D, $P < 0.001$, $n=23$, $c=56$). Ca^{2+} transient propagation spread

303 was also increased in the final 3 sec of EFS from 11 ± 0.6 to 15.4 ± 0.9 μm
304 (Figure 2 E, $P < 0.001$, $n=23$, $c=56$) and was also significantly increased, as
305 compared to control, in the post EFS period, with Ca^{2+} transients propagating an
306 average of 12.9 ± 0.6 μm (Figure 2 E, $P < 0.05$, $n=23$, $c=56$). The number of Ca^{2+}
307 firing sites in ICC-DMP was decreased significantly during the final 3 sec of EFS
308 ($P < 0.001$) and during the post-EFS period ($P < 0.001$) (Figure 2 F, $n=23$, $c=56$).
309 This is likely a result of the increased propagation spread of Ca^{2+} transients
310 during these periods, as shown in Figure 2 E. As the frequency of Ca^{2+} transients
311 increased and they propagated over longer distances, individual firing sites may
312 summate to create the increase in propagation distances observed during the
313 final seconds of EFS and post EFS. This could lead to an apparent reduction in
314 firing sites, as the underlying sites were masked by propagating Ca^{2+} waves. A
315 small increase in Ca^{2+} transient propagation velocity, that did not reach
316 significance, was also observed during the final 3 sec of EFS and during the
317 post-EFS period ($P < 0.05$, Figure 2 G, $n=23$, $c=56$).

318

319 ***EFS evoked frequency-dependent excitatory Ca^{2+} responses in ICC-DMP***

320 We examined whether the Ca^{2+} responses in ICC-DMP were dependent
321 upon the frequency of EFS. EFS was applied to muscles from 1-20 Hz (0.5ms, 5
322 sec trains). No changes in Ca^{2+} transient parameters were resolved during 1Hz
323 stimulation (Figure 3 A, $n=5$, $c=16$), although a significant increase in the
324 frequency of Ca^{2+} transients occurred in the post-EFS period (Figure 3 A, $P < 0.05$,
325 $n=5$, $c=16$). Higher EFS frequencies (5, 10 and 20 Hz) increased Ca^{2+} transients

326 significantly during EFS (final 3 sec) and during the post stimulus period (Figure
327 3 B&C). For example, 5 Hz EFS increased the firing frequency (final 3 sec) to 2.5
328 ± 0.6 events sec^{-1} , which was significantly greater than control values of 1.6 ± 0.4
329 events sec^{-1} ($P < 0.05$, $n=5$, $c=16$). EFS 5 Hz also increased Ca^{2+} transient
330 frequency during the post- EFS period to 2.5 ± 0.4 events sec^{-1} , as compared to
331 1.6 ± 0.4 events sec^{-1} in control ($P < 0.01$, $n=5$, $c=16$). During EFS, the amplitude
332 and duration of Ca^{2+} transients were not significantly changed at all frequencies
333 tested ($P > 0.05$). However, Ca^{2+} transient duration increased during the post-
334 EFS period at 5 Hz from 198 ± 10 ms to 228 ± 13.1 ms ($P < 0.05$, $n=5$, $c=16$). The
335 spread of Ca^{2+} transients was not significantly affected by 1 Hz EFS, but
336 increased significantly at 5 Hz during EFS (final 3 sec; increased from 10.1 ± 0.9
337 to 18.6 ± 2.6 μm ($P < 0.05$, $n=5$, $c=16$). At 20 Hz the spatial spread increased
338 from 8.5 ± 0.6 to 11.9 ± 1.2 μm during EFS ($P < 0.05$, $n=5$, $c=14$). The change in
339 firing frequency (% change) for each stimulus 1, 5 10 and 20 Hz was calculated
340 and plotted in Figure 3 D&E during EFS (final 3 sec, Figure 3 D) and after the
341 stimulus period (Figure 3 E). The firing of Ca^{2+} transients was dependent upon
342 the stimulus frequency during both periods (Figure 3 D&E).

343

344 **Expression of excitatory cholinergic and neurokinin receptors in ICC**

345 Excitatory neurotransmitters mediate responses by binding to specific post
346 junctional receptors. In the case of excitatory enteric neurotransmission,
347 responses have been attributed to muscarinic (M2 and M3) receptors and
348 neurokinin (NK1 and NK2) receptors expressed in small intestinal muscles (Lavin

349 et al., 1998; Stadelmann et al., 1998; Iino et al., 2004; Fausson-Pellegrini and
350 Vannucchi, 2006). In this study we sorted ICC (CopGFP-Kit⁺ cells) from small
351 intestinal muscles of Kit^{+/copGFP} mice by FACS from, as previously described
352 (Baker et al., 2016), and characterized the expression of *Chrm2* and *Chrm3*
353 transcripts and *Tacr1* and *Tacr2* transcripts. We noted higher expression of
354 *Chrm3* in ICC in comparison to *Chrm2* normalized to the housekeeping gene
355 *Gapdh* (*Chrm3*: 0.043 ± 0.001; *Chrm2*: 0.029 ± 0.002, P= 0.001, n=4). *Chrm3*
356 transcripts were also higher in ICC relative to unsorted cells (total cell population).
357 *Tacr1* was also highly expressed in ICC (*Tacr1*: 0.06 ± 0.01, n=4), and
358 expression of *Tacr2* was not resolved in ICC. Thus, the dominant receptor
359 transcripts in ICC were *Chrm3* and *Tacr1*.

360

361 ***Cholinergic regulation of Ca²⁺ transients in ICC-DMP***

362 Atropine (1 μM) decreased the frequency of basal Ca²⁺ transients from 1.9
363 ± 0.31 events sec⁻¹ to 1.2 ± 0.2 events sec⁻¹ (Figure 4 A&B, P=0.0005, n=5,
364 c=13). No significant effects on the other parameters of Ca²⁺ transients were
365 noted: amplitude (P=0.39), duration (P=0.83) or spatial spread (P=0.53; Figure 4
366 B-E; n=5, c=13). When cholinergic stimulation was initiated by exogenous
367 acetylcholine (ACh, 10 μM; in the presence of TTX, 1 μM), Ca²⁺ transients
368 increased markedly. ACh increased the frequency of Ca²⁺ transients from 0.85 ±
369 0.2 events sec⁻¹ to 1.85 ± 0.4 events sec⁻¹ (Figure 4 F&G, P=0.003, n=5, c=9),
370 and Ca²⁺ transient amplitude increased from 0.3 ± 0.04 to 0.6 ± 0.1 ΔF/F₀ (Figure
371 4 H, P=0.042, n=5, c=9). ACh increased the duration of Ca²⁺ transients from 240

372 ± 16.1 ms to 296 ± 15.3 ms (Figure 4 I, $P=0.008$, $n=5$, $c=9$). The spatial spread of
373 Ca^{2+} transients also increased in response to ACh, sometimes leading to
374 propagating Ca^{2+} waves in contrast to more spatially limited events. Spatial
375 spread increased from 7.1 ± 0.7 to 11 ± 1.3 μm (Figure 4 F&J, $P=0.017$, $n=5$,
376 $c=9$).

377

378 ***The effects of atropine on EFS evoked excitatory Ca^{2+} response in ICC-DMP***

379 Next we investigated the extent of regulation exerted by cholinergic
380 neurotransmission on Ca^{2+} transients in ICC-DMP. EFS (10Hz, for 5 sec) in the
381 presence of atropine (1 μM) resulted in a decrease in the frequency of Ca^{2+}
382 transients during stimulation (final 3 sec), from 1.7 ± 0.4 to 0.9 ± 0.2 events sec^{-1}
383 (Figure 5 A-C, $P=0.042$, $n=5$, $c=21$). Atropine also decreased the Ca^{2+} transient
384 frequency during the post stimulus period, from 2.4 ± 0.3 to 1.6 ± 0.2 events sec^{-1}
385 (Figure 5 A-C, $P=0.037$, $n=5$, $c=21$). This suggests that cholinergic
386 neurotransmission can also affect the post-stimulus excitatory period in ICC-DMP.
387 There were no significant changes in Ca^{2+} transient amplitude (Figure 5 D,
388 $P=0.46$, $P=0.19$), duration (Figure 5 E, $P=0.63$, $P=0.42$) or spatial spread (Figure
389 5 F, $P=0.44$, $P=0.56$) during either the final 3 sec of EFS or during the post-
390 stimulus period in the presence of atropine ($n=5$, $c=21$).

391

392 ***Neurokinins control over basal Ca^{2+} signaling in ICC-DMP***

393 NK1 receptors are the major neurokinin receptors expressed in ICC, and
394 results from this study confirmed previous reports (Sternini et al., 1995; Iino et al.,

395 2004). Therefore, contributions of neurokinins to EFS responses in ICC-DMP
396 were first evaluated with neurokinin 1 (NK1) receptor antagonists. RP 67580 (1
397 μM) dramatically reduced basal Ca^{2+} transients in ICC-DMP from 1.2 ± 0.2 to 0.5
398 ± 0.1 events sec^{-1} (Figure 6 A&B, $P=0.0003$, $n=11$, $c=27$). The amplitude
399 ($P=0.0039$), duration ($P=0.002$) and spatial spread ($P=0.005$) of Ca^{2+} transients
400 were also significantly depressed by RP 67580 (Figure 6 C-E $n=11$, $c=27$). SR
401 140333 (1 μM), another NK1 receptor antagonist, also inhibited basal Ca^{2+}
402 transients in ICC-DMP, reducing frequency from 0.9 ± 0.1 to 0.4 ± 0.06 events
403 sec^{-1} (Figure 6 F-J, $P=0.006$, $n=4$, $c=14$). Amplitudes ($P=0.042$) and spatial
404 spread ($P=0.003$) of Ca^{2+} transients were also significantly decreased by SR
405 140333 (Figure 6 H&J, $n=4$, $c=14$). A selective NK2 receptor antagonist, MEN
406 10376 (1 μM), had no effect on Ca^{2+} transients in ICC-DMP (i.e. frequency
407 ($P=0.081$), amplitude ($P=0.67$), duration ($P=0.24$) or spatial spread ($P=0.21$),
408 ($n=5$, $c=9$, data not shown).

409 After inhibition of Ca^{2+} transients with RP 67580 (Figure 7 A&B), carbachol
410 (CCh; 10 μM) persisted in enhancing Ca^{2+} transient firing frequency from $0.6 \pm$
411 0.2 to 2.4 ± 0.5 events sec^{-1} (Figure 7 C&D, $P=0.018$, $n=3$, $c=6$). The duration of
412 Ca^{2+} transients was increased by CCh from 183.4 ± 37.4 to 308.3 ± 18.9 ms
413 (Figure 7 F, $P=0.035$, $n=3$, $c=6$) and the spatial spread of Ca^{2+} transients was
414 also increased from 6.2 ± 1.3 to 12.1 ± 1.3 μm (Figure 7 G, $P=0.016$, $n=3$, $c=6$).
415 CCh also increased Ca^{2+} transients after treatment with SR 140333 (data not
416 shown). These results show that the effects of the NK1 antagonists were not due

417 to off-target effects, such as inhibition of IP₃-dependent signaling or Ca²⁺ release
418 from intracellular stores.

419 The observations above suggest that Ca²⁺ signaling in ICC-DMP can be
420 modulated by neurokinins via NK1, but not NK2 receptors. Regulation by
421 neurokinins was further tested by application of NK1 agonists. Substance P (1
422 μM, in the presence of TTX) increased Ca²⁺ transients significantly (Figure 8 A-
423 E); frequency increased from 1.2 ± 0.3 to 2 ± 0.3 events sec⁻¹ (Figure 8 B,
424 P=0.042, n=4, c=10), duration increased from 207 ± 15.9 to 342 ± 21.8 ms
425 (Figure 8 D, P<0.0001, n=4, c=10) and spatial spread increased from 7 ± 0.6 to
426 10.9 ± 1.2 μm (Figure 8 E, P=0.0199, n=4, c=10). A more selective NK1 agonist,
427 GR 73632 (1 μM, in the presence of TTX) also increased the frequency of Ca²⁺
428 transients from 0.3 ± 0.03 to 1.2 ± 0.2 events sec⁻¹ (Figure 8 F&G, P=0.0014, n=4,
429 c=9), but effects on amplitude (P=0.92), duration (P=0.78) or spatial spread
430 (P=0.42) were not changed significantly (Figure 8 H-J, n=4, c=9). These data
431 suggest that neurokinins are released tonically in small intestinal muscles, and
432 responses of ICC-DMP to neurokinins are mediated largely by NK1 receptors.

433

434 ***The effects of RP 67580 on Ca²⁺ responses evoked by EFS in ICC-DMP***

435 We also tested whether NK1 receptors mediate Ca²⁺ responses in ICC-
436 DMP evoked by EFS. RP 67580 (1 μM; Figure 9 A&B) caused a dramatic
437 decrease in the Ca²⁺ responses to EFS (Figure 9 C-F). The frequency of Ca²⁺
438 transients during the final 3 sec of EFS period was reduced from 1.5 ± 0.3 to 0.2
439 ± 0.17 events sec⁻¹ (Figure 9 C, P=0.0015, n=4, c=11). During the post EFS

440 period, the frequency of Ca^{2+} transients was also significantly reduced from $1.8 \pm$
441 0.3 to 0.1 ± 0.05 events sec^{-1} (Figure 9 C, $P=0.002$, $n=4$, $c=11$). Ca^{2+} transient
442 amplitude, duration and spatial spread during the final 3 sec EFS and post EFS
443 periods were also inhibited (Figure 9 D-F, $n=4$, $c=11$).

444 When cholinergic and NK1 receptors were both antagonized by adding
445 both atropine ($1 \mu\text{M}$) and RP 67580 ($1 \mu\text{M}$), pronounced inhibition of Ca^{2+}
446 transients persisted during the final 3 sec of EFS and during the post stimulus
447 period, as shown in Figure 10 A-F ($n=4$, $c=20$).

448

449 ***Cholinergic and neurokinin mediated excitatory responses after blocking***
450 ***nitrenergic and purinergic transmission***

451 Nitrenergic and purinergic antagonists N-omega-nitro-L-arginine (L-NNA,
452 $100 \mu\text{M}$) and MRS 2500 ($1 \mu\text{M}$) were used to examine excitatory neural
453 regulation of Ca^{2+} transients in ICC-DMP after blocking major inhibitory pathway
454 of neurotransmission. In the presence of L-NNA, MRS 2500 and atropine ($1 \mu\text{M}$)
455 Ca^{2+} transient frequency (Figure 11 C, $P=0.29$, $n=7$, $c=26$), amplitude (Figure 11
456 D, $P=0.57$, $n=7$, $c=26$) and spatial spread (Figure 11 F, $P=0.3$, $n=7$, $c=26$) in the
457 final 3 sec period were not significantly affected. Ca^{2+} transient duration
458 decreased significantly from 266 ± 14.15 to 199 ± 18.9 ms (Figure 11 E, $P=0.007$,
459 $n=7$, $c=26$) in the final 3 sec period. In the presence of L-NNA, MRS 2500 and
460 atropine, Ca^{2+} transients in the post-stimulus period were not reduced in
461 amplitude (Figure 11 D, $P=0.64$, $n=7$, $c=26$) or spatial spread (Figure 11 F,
462 $P=0.088$, $n=7$, $c=26$). However, the frequency of Ca^{2+} transients was reduced

463 during the post-stimulus period from 2.6 ± 0.25 to 1.9 ± 0.2 events sec^{-1} (Figure
464 11 C, $P=0.03$, $n=7$, $c=26$) and duration decreased from 237 ± 11.6 to 177 ± 11.9
465 ms (Figure 11 E, $P=0.0008$, $n=7$, $c=26$).

466 We next examined the neurokinin input into EFS-mediated excitatory
467 responses in ICC-DMP in the presence of blockers of nitroergic and purinergic
468 neurotransmission. With L-NNA, MRS 2500 and RP 67580 present, responses to
469 EFS were significantly reduced in amplitude, duration and spatial spread of Ca^{2+}
470 transients during the final 3 sec of EFS (Figure 12 D-F, $n=4$, $c=13$). The
471 amplitude decreased from 1.4 ± 0.2 to $0.42 \pm 0.8 \Delta F/F_0$ ($P=0.002$, Figure 12 D,
472 $n=4$, $c=13$), the duration decreased from 214.4 ± 16.9 to 122 ± 22 ms ($P=0.004$,
473 Figure 12 E, $n=4$, $c=13$) and the spatial spread decreased from 15.4 ± 3.2 to 5.8
474 $\pm 1 \mu\text{m}$ ($P=0.029$, Figure 12 F, $n=4$, $c=13$). Overall the frequency of Ca^{2+}
475 transients in the final 3 sec of the EFS period was not significantly affected
476 (Figure 12 A-C, $P=0.21$, $n=4$, $c=13$). In the presence of L-NNA, MRS 2500 and
477 RP 67580, the frequency of Ca^{2+} transients in the post-EFS period was
478 significantly reduced from 1.8 ± 0.3 to 0.4 ± 0.1 events sec^{-1} (Figure 12 C,
479 $P=0.006$, $n=4$, $c=13$). The amplitude of Ca^{2+} transients during this period was not
480 significantly affected (Figure 12 D, $P=0.059$, $n=4$, $c=13$), but the duration of Ca^{2+}
481 transients was reduced from 237 ± 23.9 to 121 ± 19.7 ms (Figure 12 E, $P=0.0029$,
482 $n=4$, $c=13$), and spatial spread decreased from 12.61 ± 1.6 to $6.8 \pm 1.2 \mu\text{m}$
483 (Figure 12 F, $P=0.014$, $n=4$, $c=13$).

484 Next we inhibited cholinergic and neurokinin transmission with atropine
485 and RP 67580 in the presence of L-NNA and MRS 2500. Under these conditions

486 all Ca^{2+} transients were significantly diminished across all parameters tabulated,
487 as shown in (Fig.13 A-F n=5, c=32).

488

489

490 **Discussion**

491 Innervation of GI muscles by enteric motor nerves and the integrated firing
492 of these neurons is essential for generating archetypal motility patterns (Spencer
493 et al., 2016). ICC are innervated by enteric motor neurons, and their responses
494 to neurotransmitters contribute to complex post-junctional responses of the SIP
495 syncytium (Ward et al., 2000; Iino et al., 2004). In the case of the small intestine
496 ICC-DMP are an intramuscular type of ICC that are closely associated with and
497 innervated by motor neurons (Rumessen *et al.*, 1992; Zhou & Komuro, 1992;
498 Wang *et al.*, 2003b; Iino *et al.*, 2004; Ward *et al.*, 2006). We recently described
499 the properties of spontaneous Ca^{2+} transients that occur in the absence of
500 extrinsic stimuli in these cells (Baker et al., 2016). In the present study we
501 investigated the effects of excitatory enteric motor neurotransmission on Ca^{2+}
502 transients in ICC-DMP, because these events mediate activation of CaCC, the
503 ion channels responsible for the electrophysiological post-junctional excitatory
504 responses to nerve stimulation in small intestinal muscles (Zhu et al., 2011). EFS
505 of intrinsic neurons resulted in three-component effects on Ca^{2+} transients: a
506 brief inhibitory period (about 2s), a period of escape from inhibition during
507 sustained EFS, and a period of strong excitation after cessation of the stimuli
508 (post-stimulus or 'rebound' excitation). The complexity of these responses is
509 likely due to the fact that the enteric nervous system contains both inhibitory and
510 excitatory motor neurons (Furness, 2012), and EFS can be expected to activate
511 both classes of neurons.

512 In the mouse small intestine, the neurokinin component of the excitatory
513 neural inputs to ICC-DMP was dominant. Our experiments also suggest that
514 tonic release of neurokinins and binding to NK1 receptors is responsible for
515 significant drive in generating the Ca²⁺ transients observed under basal
516 conditions in ICC-DMP (Baker et al., 2016). Thus, the Ca²⁺ transients observed
517 in the absence of applied stimuli are not 'spontaneous' and do not appear to be
518 driven intrinsically within ICC-DMP. Excitatory neurotransmitters greatly
519 increased Ca²⁺ transients in ICC-DMP, and this mechanism likely underlies a
520 portion of the post-junctional electrophysiological response to excitatory neural
521 regulation (Zhu et al., 2011; Zhu et al., 2015).

522 ICC-DMP are plentiful and in close contact with varicosities of enteric
523 motor neurons in the deep muscular plexus region of the small intestine
524 (Rumessen et al., 1992; Zhou and Komuro, 1992). We confirmed that ICC
525 express receptors required for excitatory motor neurotransmission (e.g.
526 muscarinic and neurokinin receptors), and transcripts for M3 (*Chrm3*) and NK1
527 (*Tacr1*) were enriched in ICC-DMP vs. unsorted cells. However, transcripts of
528 *Chrm2* were also present, suggesting these receptors and coupling to effectors
529 via Gi/Go may also have a role in transduction or modulation of excitatory
530 neurotransmission. Our findings are consistent with previous studies showing
531 muscarinic receptors and NK1 receptor expression in ICC with
532 immunohistochemical techniques (Sternini et al., 1995; Vannucchi et al., 1997;
533 Stadelmann et al., 1998; Iino et al., 2004; Iino and Nojyo, 2006; Ward et al.,
534 2006; Sanders et al., 2014b).

535 This study demonstrates that ICC-DMP receive and transduce excitatory
536 neural inputs in the small bowel. Previous studies predicted this finding from
537 morphological observations (Rumessen et al., 1992; Zhou and Komuro, 1992;
538 Wang et al., 2003a; Iino et al., 2004; Faussonne-Pellegrini, 2006; Shimizu et al.,
539 2008) and by showing that cholinergic excitatory neural responses develop in
540 phase with the development of ICC-DMP and blocking Kit receptors causes
541 parallel loss of ICC and cholinergic neural responses (Ward et al., 2006).
542 Excitatory neurotransmission caused PKC ϵ translocation in ICC-DMP that was
543 blocked by atropine (Wang et al., 2003b), demonstrating functional cholinergic
544 innervation and muscarinic responses in these cells. ACh binding to M3
545 receptors can enhance Ca²⁺ release in ICC-DMP via generation of inositol 1,4,5-
546 trisphosphate (IP₃) which activates Ca²⁺ release from the endoplasmic reticulum
547 (ER). All of the molecular components of this pathway are expressed in ICC, as
548 shown by transcriptome analyses (Chen et al., 2007; Lee et al., 2017). Previous
549 direct observation of ICC-DMP *in situ* has shown that Ca²⁺ transients are due to
550 Ca²⁺ release from intracellular stores (e.g. ER), mediated, in part, by IP₃R (Baker
551 et al., 2016). Increasing Ca²⁺ release in ICC leads to activation of CaCC, and the
552 inward current generated by thousands of ICC-DMP in whole muscles would
553 provide a net depolarizing influence that would summate with slow wave
554 depolarizations, increase the likelihood of action potentials being generated
555 during the plateau phase of slow waves (i.e. period of peak depolarization), and
556 enhance the amplitude of phasic contractions (Zhu et al., 2011).

557 While our observations suggest innervation and contributions from
558 cholinergic nerves to post-junctional excitatory responses, our data also suggest
559 that neurokinins are the dominant excitatory neurotransmitters affecting Ca^{2+}
560 transients in ICC-DMP in the mouse small intestine. ICC-DMP are closely
561 associated with substance P containing nerve fibers, and ICC-DMP express NK1
562 receptors (Iino et al., 2004; Fausone-Pellegrini, 2006; Shimizu et al., 2008)
563 which is consistent with our observation that excitatory transmission to ICC-DMP
564 was mediated through NK1 receptors. Previous studies have shown that
565 exposure of small intestinal muscles to substance P or stimulation of motor
566 neurons causes internalization of NK1 receptors in ICC (Lavin et al., 1998; Iino et
567 al., 2004). Our experiments showed that two NK1 receptor antagonists greatly
568 attenuated basal Ca^{2+} transients and suppressed responses of ICC-DMP to EFS.
569 The strong inhibitory effects of NK1 antagonists on Ca^{2+} transients could possibly
570 be due to off-target effects on Ca^{2+} stores or Ca^{2+} release mechanisms, however
571 non-specific effects do not appear to be significant because responses to CCh on
572 Ca^{2+} transients were intact in the presence of the NK1 antagonist, RP 67580.
573 Taken together these findings support the importance of neurokinin signaling in
574 shaping motility patterns in the small intestine.

575 The degree to which basal Ca^{2+} transients were affected by NK1
576 antagonists in the present study was somewhat surprising. These results
577 suggest ongoing release of neurokinins (i.e. tonic excitation), similar in concept to
578 the tonic inhibition phenomena observed in many GI muscles (Wood, 1972;
579 Lyster et al., 1995). Although this phenomenon has not been described

580 previously in the small intestine, tonic activation of NK1 receptors has been
581 proposed in other systems (Henry et al., 1999; Jasmin et al., 2002). In the
582 present study attenuation of Ca^{2+} transients by the NK1 receptor antagonists may
583 be caused by continuous release of neurokinins or persistence of the ligand in
584 the spaces between motor nerve varicosities and ICC-DMP.

585 The enhanced relative reliance on neurokinins for excitatory effects may
586 be due, in part, to the high expression of NK1 receptors by ICC-DMP which does
587 not appear to be true for intramuscular ICC in the colon (Lee et al., 2017). NK1
588 receptors also couple to cellular responses through activation of phospholipase C
589 and generation of IP_3 (Steinhoff et al., 2014). Thus, there is a signaling pathway
590 available for the enhancement of Ca^{2+} transients in ICC-DMP. However, it
591 should also be noted that transfection of neurokinin receptors in model cells has
592 also been associated with activation of adenylate cyclase and production of
593 cAMP (Steinhoff et al., 2014), a pathway not typically linked to enhanced release
594 of Ca^{2+} . Generation of cAMP and stimulation of cAMP-dependent protein kinase
595 is known to enhance Ca^{2+} sequestration into stores by phosphorylation of
596 phospholamban (highly expressed in ICC; (Lee et al., 2017) and stimulation of
597 SERCA (Stammers et al., 2015). Perhaps increased loading of Ca^{2+} stores
598 contributes to augmentation of Ca^{2+} transient amplitude and spatial spread by
599 neurokinins, and enhancing the rate of recovery of Ca^{2+} into stores after a
600 release event reduces the time required for a given store to generate another
601 Ca^{2+} transient.

602 In summary, this study supports the idea that significant neural regulation
603 occurs in the intramuscular class of ICC in the small intestine (ICC-DMP). As
604 discussed above, much of the excitatory response was mediated through NK1
605 receptors that are expressed largely by ICC-DMP (Sternini et al., 1995;
606 Vannucchi et al., 1997; Iino et al., 2004). Responses to EFS were attenuated by
607 NK1 antagonists. Previous studies have shown that electrophysiological
608 responses in ICC-DMP are linked to Ca^{2+} release events (Zhu et al., 2011; Zhu et
609 al., 2015), suggesting that Ca^{2+} transients in ICC-DMP couple to generation of
610 inward currents and depolarizing effects on the SIP syncytium. NK2 receptors,
611 expressed largely by SMCs (Cipriani et al., 2011), were apparently not involved
612 in responses of ICC-DMP to neurokinins released from nerve terminals, because
613 an NK2 antagonist had no effect on responses. The effectiveness of neurokinins
614 as neurotransmitters in the *tunica muscularis* of the small intestine may be
615 spatially confined by concentrations achieved in post-junctional spaces to a
616 subset of neurokinin receptors expressed by ICC-DMP.
617
618
619

620 **References**

621

- 622 Baker SA, Hennig GW, Salter AK, Kurahashi M, Ward SM, Sanders KM (2013)
623 Distribution and Ca(2+) signalling of fibroblast-like (PDGFR(+)) cells in the
624 murine gastric fundus. *J Physiol* 591:6193-6208.
- 625 Baker SA, Drumm BT, Saur D, Hennig GW, Ward SM, Sanders KM (2016)
626 Spontaneous Ca(2+) transients in interstitial cells of Cajal located within the
627 deep muscular plexus of the murine small intestine. *J Physiol* 594:3317-3338.
- 628 Blair PJ, Bayguinov Y, Sanders KM, Ward SM (2012) Interstitial cells in the primate
629 gastrointestinal tract. *Cell Tissue Res* 350:199-213.
- 630 Burns AJ, Lomax AE, Torihashi S, Sanders KM, Ward SM (1996) Interstitial cells of
631 Cajal mediate inhibitory neurotransmission in the stomach. *Proc Natl Acad*
632 *Sci U S A* 93:12008-12013.
- 633 Chen H, Ordog T, Chen J, Young DL, Bardsley MR, Redelman D, Ward SM, Sanders KM
634 (2007) Differential gene expression in functional classes of interstitial cells of
635 Cajal in murine small intestine. *Physiol Genomics* 31:492-509.
- 636 Cipriani G, Serboiu CS, Gherghiceanu M, Faussonne-Pellegrini MS, Vannucchi MG
637 (2011) NK receptors, Substance P, Ano1 expression and ultrastructural
638 features of the muscle coat in Cav-1(-/-) mouse ileum. *J Cell Mol Med*
639 15:2411-2420.
- 640 Daniel EE, Posey-Daniel V (1984) Neuromuscular structures in opossum esophagus:
641 role of interstitial cells of Cajal. *Am J Physiol* 246:G305-315.
- 642 Daniel EE, Wang YF (1999) Gap junctions in intestinal smooth muscle and
643 interstitial cells of Cajal. *Microsc Res Tech* 47:309-320.
- 644 Daniel EE, Wang YF, Cayabyab FS (1998) Role of gap junctions in structural
645 arrangements of interstitial cells of Cajal and canine ileal smooth muscle. *Am*
646 *J Physiol* 274:G1125-1141.
- 647 De Schepper HU, De Winter BY, Seerden TC, Herman AG, Pelckmans PA, De Man JG
648 (2005) Functional characterisation of tachykinin receptors in the circular
649 muscle layer of the mouse ileum. *Regul Pept* 130:105-115.
- 650 Drumm BT, Hennig GW, Battersby MJ, Cunningham EK, Sung TS, Ward SM, Sanders
651 KM, Baker SA (2017) Clustering of Ca²⁺ transients in interstitial cells of Cajal
652 defines slow wave duration. *J Gen Physiol* 149:703-725.
- 653 Faussonne-Pellegrini MS (2006) Relationships between neurokinin receptor-
654 expressing interstitial cells of Cajal and tachykininergic nerves in the gut. *J*
655 *Cell Mol Med* 10:20-32.
- 656 Faussonne-Pellegrini MS, Vannucchi MG (2006) Substance P and Neurokinin 1
657 receptor - expression is affected in the ileum of mice with mutation in the W
658 locus. *J Cell Mol Med* 10:511-518.
- 659 Furness JB (2012) The enteric nervous system and neurogastroenterology. *Nat Rev*
660 *Gastroenterol Hepatol* 9:286-294.
- 661 Gomez-Pinilla PJ, Gibbons SJ, Bardsley MR, Lorincz A, Pozo MJ, Pasricha PJ, Van de
662 Rijn M, West RB, Sarr MG, Kendrick ML, Cima RR, Dozois EJ, Larson DW,
663 Ordog T, Farrugia G (2009) Ano1 is a selective marker of interstitial cells of

- 664 Cajal in the human and mouse gastrointestinal tract. *Am J Physiol*
665 Gastrointest Liver Physiol 296:G1370-1381.
- 666 Goyal RK (2016) CrossTalk opposing view: Interstitial cells are not involved and
667 physiologically important in neuromuscular transmission in the gut. *J Physiol*
668 594:1511-1513.
- 669 Goyal RK, Chaudhury A (2010) Mounting evidence against the role of ICC in
670 neurotransmission to smooth muscle in the gut. *Am J Physiol Gastrointest*
671 Liver Physiol 298:G10-13.
- 672 Henry JL, Yashpal K, Pitcher GM, Chabot J, Coderre TJ (1999) Evidence for tonic
673 activation of NK-1 receptors during the second phase of the formalin test in
674 the Rat. *J Neurosci* 19:6588-6598.
- 675 Holzer P, Holzer-Petsche U (2001) Tachykinin receptors in the gut: physiological
676 and pathological implications. *Curr Opin Pharmacol* 1:583-590.
- 677 Huizinga JD et al. (2014) The origin of segmentation motor activity in the intestine.
678 *Nat Commun* 5:3326.
- 679 Iino S, Nojyo Y (2006) Muscarinic M(2) acetylcholine receptor distribution in the
680 guinea-pig gastrointestinal tract. *Neuroscience* 138:549-559.
- 681 Iino S, Ward SM, Sanders KM (2004) Interstitial cells of Cajal are functionally
682 innervated by excitatory motor neurones in the murine intestine. *J Physiol*
683 556:521-530.
- 684 Iino S, Horiguchi K, Horiguchi S, Nojyo Y (2009) c-Kit-negative fibroblast-like cells
685 express platelet-derived growth factor receptor alpha in the murine
686 gastrointestinal musculature. *Histochem Cell Biol* 131:691-702.
- 687 Jasmin L, Tien D, Weinshenker D, Palmiter RD, Green PG, Janni G, Ohara PT (2002)
688 The NK1 receptor mediates both the hyperalgesia and the resistance to
689 morphine in mice lacking noradrenaline. *Proc Natl Acad Sci U S A* 99:1029-
690 1034.
- 691 Klein S, Seidler B, Kettenberger A, Sibaev A, Rohn M, Feil R, Allescher HD,
692 Vanderwinden JM, Hofmann F, Schemann M, Rad R, Storr MA, Schmid RM,
693 Schneider G, Saur D (2013) Interstitial cells of Cajal integrate excitatory and
694 inhibitory neurotransmission with intestinal slow-wave activity. *Nat*
695 *Commun* 4:1630.
- 696 Komuro T (2006) Structure and organization of interstitial cells of Cajal in the
697 gastrointestinal tract. *J Physiol* 576:653-658.
- 698 Komuro T, Seki K, Horiguchi K (1999) Ultrastructural characterization of the
699 interstitial cells of Cajal. *Arch Histol Cytol* 62:295-316.
- 700 Langton P, Ward SM, Carl A, Norell MA, Sanders KM (1989) Spontaneous electrical
701 activity of interstitial cells of Cajal isolated from canine proximal colon. *Proc*
702 *Natl Acad Sci U S A* 86:7280-7284.
- 703 Lavin ST, Southwell BR, Murphy R, Jenkinson KM, Furness JB (1998) Activation of
704 neurokinin 1 receptors on interstitial cells of Cajal of the guinea-pig small
705 intestine by substance P. *Histochem Cell Biol* 110:263-271.
- 706 Lee HT, Hennig GW, Fleming NW, Keef KD, Spencer NJ, Ward SM, Sanders KM, Smith
707 TK (2007) The mechanism and spread of pacemaker activity through
708 myenteric interstitial cells of Cajal in human small intestine.
709 *Gastroenterology* 132:1852-1865.

- 710 Lee MY, Ha SE, Park C, Park PJ, Fuchs R, Wei L, Jorgensen BG, Redelman D, Ward SM,
711 Sanders KM, Ro S (2017) Transcriptome of interstitial cells of Cajal reveals
712 unique and selective gene signatures. *PLoS One* 12:e0176031.
- 713 Lyster DJ, Bywater RA, Taylor GS (1995) Neurogenic control of myoelectric
714 complexes in the mouse isolated colon. *Gastroenterology* 108:1371-1378.
- 715 Mitsui R (2011) Immunohistochemical analysis of substance P-containing neurons
716 in rat small intestine. *Cell Tissue Res* 343:331-341.
- 717 Ordog T, Ward SM, Sanders KM (1999) Interstitial cells of cajal generate electrical
718 slow waves in the murine stomach. *J Physiol* 518 (Pt 1):257-269.
- 719 Rumessen JJ, Mikkelsen HB, Thuneberg L (1992) Ultrastructure of interstitial cells of
720 Cajal associated with deep muscular plexus of human small intestine.
721 *Gastroenterology* 102:56-68.
- 722 Sanders KM, Ward SM (2006) Interstitial cells of Cajal: a new perspective on smooth
723 muscle function. *J Physiol* 576:721-726.
- 724 Sanders KM, Ward SM, Koh SD (2014a) Interstitial cells: regulators of smooth
725 muscle function. *Physiol Rev* 94:859-907.
- 726 Sanders KM, Koh SD, Ro S, Ward SM (2012) Regulation of gastrointestinal motility--
727 insights from smooth muscle biology. *Nat Rev Gastroenterol Hepatol* 9:633-
728 645.
- 729 Sanders KM, Salter AK, Hennig GW, Koh SD, Perrino BA, Ward SM, Baker SA (2014b)
730 Responses to enteric motor neurons in the gastric fundus of mice with
731 reduced intramuscular interstitial cells of cajal. *J Neurogastroenterol Motil*
732 20:171-184.
- 733 Seki K, Komuro T (2001) Immunocytochemical demonstration of the gap junction
734 proteins connexin 43 and connexin 45 in the musculature of the rat small
735 intestine. *Cell Tissue Res* 306:417-422.
- 736 Shimizu Y, Matsuyama H, Shiina T, Takewaki T, Furness JB (2008) Tachykinins and
737 their functions in the gastrointestinal tract. *Cell Mol Life Sci* 65:295-311.
- 738 Spencer NJ, Dinning PG, Brookes SJ, Costa M (2016) Insights into the mechanisms
739 underlying colonic motor patterns. *J Physiol* 594:4099-4116.
- 740 Stadelmann AM, Walgenbach-Telford S, Telford GL, Koch TR (1998) Distribution of
741 muscarinic receptor subtypes in rat small intestine. *J Surg Res* 80:320-325.
- 742 Stammers AN, Susser SE, Hamm NC, Hlynsky MW, Kimber DE, Kehler DS, Duhamel
743 TA (2015) The regulation of sarco(endo)plasmic reticulum calcium-ATPases
744 (SERCA). *Can J Physiol Pharmacol* 93:843-854.
- 745 Steinhoff MS, von Mentzer B, Geppetti P, Pothoulakis C, Bunnett NW (2014)
746 Tachykinins and their receptors: contributions to physiological control and
747 the mechanisms of disease. *Physiol Rev* 94:265-301.
- 748 Sternini C, Su D, Gamp PD, Bunnett NW (1995) Cellular sites of expression of the
749 neurokinin-1 receptor in the rat gastrointestinal tract. *J Comp Neurol*
750 358:531-540.
- 751 van Helden DF, Imtiaz MS (2003) Ca²⁺ phase waves: a basis for cellular pacemaking
752 and long-range synchronicity in the guinea-pig gastric pylorus. *J Physiol*
753 548:271-296.

- 754 Vannucchi MG, De Giorgio R, Faussonne-Pellegrini MS (1997) NK1 receptor
755 expression in the interstitial cells of Cajal and neurons and tachykinins
756 distribution in rat ileum during development. *J Comp Neurol* 383:153-162.
- 757 Wang XY, Paterson C, Huizinga JD (2003a) Cholinergic and nitrenergic innervation of
758 ICC-DMP and ICC-IM in the human small intestine. *Neurogastroenterol Motil*
759 15:531-543.
- 760 Wang XY, Ward SM, Gerthoffer WT, Sanders KM (2003b) PKC-epsilon translocation
761 in enteric neurons and interstitial cells of Cajal in response to muscarinic
762 stimulation. *Am J Physiol Gastrointest Liver Physiol* 285:G593-601.
- 763 Ward SM, McLaren GJ, Sanders KM (2006) Interstitial cells of Cajal in the deep
764 muscular plexus mediate enteric motor neurotransmission in the mouse
765 small intestine. *J Physiol* 573:147-159.
- 766 Ward SM, Burns AJ, Torihashi S, Sanders KM (1994) Mutation of the proto-oncogene
767 c-kit blocks development of interstitial cells and electrical rhythmicity in
768 murine intestine. *J Physiol* 480 (Pt 1):91-97.
- 769 Ward SM, Beckett EA, Wang X, Baker F, Khoyi M, Sanders KM (2000) Interstitial cells
770 of Cajal mediate cholinergic neurotransmission from enteric motor neurons. *J*
771 *Neurosci* 20:1393-1403.
- 772 Wood JD (1972) Excitation of intestinal muscle by atropine, tetrodotoxin, and
773 xylocaine. *Am J Physiol* 222:118-125.
- 774 Zhou DS, Komuro T (1992) Interstitial cells associated with the deep muscular
775 plexus of the guinea-pig small intestine, with special reference to the
776 interstitial cells of Cajal. *Cell Tissue Res* 268:205-216.
- 777 Zhu MH, Sung TS, O'Driscoll K, Koh SD, Sanders KM (2015) Intracellular Ca²⁺
778 release from endoplasmic reticulum regulates slow wave currents and
779 pacemaker activity of interstitial cells of Cajal. *Am J Physiol Cell Physiol*
780 308:C608-620.
- 781 Zhu MH, Kim TW, Ro S, Yan W, Ward SM, Koh SD, Sanders KM (2009) A Ca²⁺-
782 activated Cl⁻ conductance in interstitial cells of Cajal linked to slow wave
783 currents and pacemaker activity. *J Physiol* 587:4905-4918.
- 784 Zhu MH, Sung IK, Zheng H, Sung TS, Britton FC, O'Driscoll K, Koh SD, Sanders KM
785 (2011) Muscarinic activation of Ca²⁺-activated Cl⁻ current in interstitial cells
786 of Cajal. *J Physiol* 589:4565-4582.
- 787

788

789

790

791

792 **Figure legends**

793

794 **Figure 1. ICC-DMP Ca²⁺ transient responses to nerve stimulation.**

795 **A** Time-lapse montage showing post-junctional Ca²⁺ responses to EFS (10 Hz;
796 0.5 ms duration; 5 sec) on an ICC-DMP *in situ*. An image of the GCaMP3 signal
797 in the cell is shown in the leftmost panel. Scale bar is 25 μm and pertains to all
798 panels. A color-coded overlay and calibration scale was imported to depict
799 fluorescence intensity (F/F_0) and enhance visualization of Ca²⁺ sites. Low
800 fluorescence areas are indicated in dark blue or black. High intensity
801 fluorescence areas are indicated in red and orange. The 'pre stimulation' panel
802 shows a summed image of Ca²⁺ activity within the cell for 5 seconds before the
803 onset of EFS, Ca²⁺ firing sites are marked with red asterisks. Panels showing the
804 summed Ca²⁺ activity for the initial 2 seconds of EFS, the final 3 seconds of EFS
805 and 5 seconds post EFS are also shown. **B** Representative ST map of Ca²⁺
806 transients in ICC-DMP shown in panel A. EFS duration is indicated by the
807 dashed white box. The firing activities of 3 sites highlighted on the ST map are
808 plotted in panel **C**, and the timing of EFS is indicated by the dashed red box.

809

810 **Figure 2. Effects of nerve stimulation (EFS) on Ca²⁺ transients in ICC-DMP.**

811 **A** Representative traces representing Ca²⁺ transients in ICC-DMP in response to
812 EFS (10Hz; 5 sec). The period of EFS is indicated by the red arrowed line).
813 Excitatory responses during the final 3 sec of EFS, indicated by the dashed blue
814 box, and during the post EFS period (5 sec), highlighted by the green box. **B – G**

815 Summary data quantifying the effects of EFS on ICC-DMP: Ca^{2+} transient
816 frequency (*E*), amplitude (*F*), duration (*G*), spatial spread (*H*), number of Ca^{2+}
817 firing sites (*I*) and Ca^{2+} transient velocity (*J*) were analyzed and shown; $n = 23$, c
818 = 56. All statistical analyses shown are compared to control values. $ns = P > 0.05$,
819 * = $P < 0.05$, ** = $P < 0.01$, *** = $P < 0.001$, **** = $P < 0.0001$.

820

821 **Figure 3. Frequency dependence of Ca^{2+} transient responses to EFS.**

822 **A** Summary data showing the excitatory effects of EFS (1Hz for 5 sec) on Ca^{2+}
823 transients in ICC-DMP during the final 3s of EFS and during the post-stimulus
824 period (5s following termination of EFS). Ca^{2+} transient parameters shown
825 include: frequency (sec^{-1}), amplitude ($\Delta F/F_0$), duration (FDHM) and spatial spread
826 (μm) of Ca^{2+} transients. **B** Summary data showing the effects of EFS (5Hz; 5
827 sec) on Ca^{2+} transient parameters. **C** Summary data showing the effects of EFS
828 (20Hz; 5 sec) on Ca^{2+} transient parameters. **D** Percentage (%) change of Ca^{2+}
829 transient firing frequency at all frequencies of EFS tested (1-20 Hz; net
830 percentage change normalized to control) during the final 3 sec of EFS and
831 during the post-stimulus period **E**. Note the frequency dependent effects of EFS
832 on Ca^{2+} transient responses. Summary data in all panels shows the include 5
833 secs before EFS, the final 3 secs during EFS and 5 seconds post-EFS. $ns = P >$
834 0.05 , * = $P < 0.05$, ** = $P < 0.01$.

835

836

837

838

839 **Figure 4. Modulation of basal Ca²⁺ transients by cholinergic input.**

840 **A** Representative ST maps showing the effects of atropine (1 μM) on basal Ca²⁺
841 transient activity in ICC-DMP. **B – E** Summary graphs showing the effect of
842 atropine on the frequency (*B*), amplitude (*C*), duration (*D*) and spatial spread (*E*)
843 of basal Ca²⁺ transients in ICC-DMP (n=5, c=13). **F** Representative ST maps
844 showing the effects of ACh (10 μM; in the presence of TTX) on Ca²⁺ transients in
845 ICC-DMP. **G – J** Summary graphs showing the effect of ACh (in the presence of
846 TTX) on the frequency (*G*), amplitude (*H*), duration (*I*) and spatial spread (*J*) of
847 Ca²⁺ transients in ICC-DMP (n=5, c=9). ns = P > 0.05, * = P < 0.05, ** = P < 0.01,
848 *** = P < 0.001.

849

850 **Figure 5. Effects of atropine on Ca²⁺ transient responses to EFS.**

851 **A - B** Representative ST maps showing the effects of atropine (1 μM) on Ca²⁺
852 transients in ICC-DMP in response to nerve stimulation (EFS; 10 Hz; 5 sec;
853 indicated by the red line and dotted white box in ST maps). **C – F** Summary data
854 showing the effects of atropine (1 μM) on Ca²⁺ transients during EFS: frequency
855 (*C*), amplitude (*D*), duration (*E*) and spatial spread (*F*) in ICC-DMP during control
856 conditions, during the excitatory period of EFS (final 3 sec), and during the post
857 EFS period (5 sec), n=5, c=21. ns = P > 0.05, * = P < 0.05, ** = P < 0.01.

858

859 **Figure 6. Effects of neurokinin receptor (NK1) antagonists on basal Ca²⁺**
860 **transients.**

861 **A** Representative ST maps showing the inhibitory effects of the NK1 receptor
862 antagonist, RP 67580 (1 μ M), on Ca^{2+} transients in ICC-DMP. **B – E** Summary
863 graphs showing the effects of RP 67580 on the frequency (*B*), amplitude (*C*),
864 duration (*D*) and spatial spread (*E*) of Ca^{2+} transients in ICC-DMP ($n=11$, $c=27$).
865 **F** Representative ST maps showing the inhibitory effects of the NK1 receptor
866 antagonist, SR 140333 (1 μ M), on Ca^{2+} transients in ICC-DMP. **G – J** Summary
867 graphs showing the effects of 1 μ M SR 140333 on the frequency (*G*), amplitude
868 (*H*), duration (*I*) and spatial spread (*J*) of Ca^{2+} transients in ICC-DMP ($n=4$, $c=14$).
869 $ns = P > 0.05$, $* = P < 0.05$, $** = P < 0.01$, $*** = P < 0.001$.

870

871 **Figure 7. NK1 antagonist does not interfere with Ca^{2+} release mechanisms.**

872 **A - B** Representative ST maps showing the effect of the NK1 antagonist RP
873 67580 (1 μ M) on Ca^{2+} transients in ICC-DMP. **C** ST map showing that in the
874 presence of RP 67580, CCh (10 μ M) strongly activates Ca^{2+} transients. **D – G**
875 Summary graphs showing the effects of CCh on Ca^{2+} transient parameters:
876 frequency (*D*), amplitude (*E*), duration (*F*) and spatial spread (*G*) in ICC-DMP in
877 the presence of RP 67580 ($n=3$, $c=6$). $* = P < 0.05$.

878

879 **Figure 8. Neurokinin receptor (NK1) agonists activate Ca^{2+} transients.**

880 **A** Representative ST maps showing the excitatory effects of substance P (1 μ M;
881 in the presence of TTX) on Ca^{2+} transients in ICC-DMP. **B – E** Summary graphs
882 showing the effects of substance P (in the presence of TTX) on the frequency (*B*),
883 amplitude (*C*), duration (*D*) and spatial spread (*E*) of Ca^{2+} transients in ICC-DMP.

884 **F** Representative ST maps showing the excitatory effects of the NK1 receptor
885 agonist GR 73632 (1 μ M; in the presence of TTX) on Ca^{2+} transients in ICC-DMP
886 (n=4, c=10). **G – J** Summary graphs quantifying the effect of GR 73632 on the
887 frequency (*G*), amplitude (*H*), duration (*I*) and spatial spread (*J*) of basal Ca^{2+}
888 transient activity in ICC-DMP (n=4, c=9). ns = $P > 0.05$, * = $P < 0.05$, ** = $P <$
889 0.01, **** = $P < 0.0001$.

890

891 **Figure 9. Effects of NK1 receptor antagonist on Ca^{2+} transient responses to**
892 **EFS.**

893 **A - B** Representative ST maps showing the inhibitory effects of NK1 antagonist,
894 RP 67580 (1 μ M), on Ca^{2+} transients in response to nerve stimulation (EFS at 10
895 Hz for 5 sec; indicated by the red line and dotted white box in ST maps). **C – F**
896 Summary data showing the inhibitory effects of RP 67580 (1 μ M) on Ca^{2+}
897 transient frequency (*C*), amplitude (*D*), duration (*E*) and spatial spread (*F*) in ICC-
898 DMP during the control period, during the final 3 sec of EFS, and during the post-
899 EFS period (5 sec), n=4, c=11. Note: RP 67580 reduced all Ca^{2+} transient
900 parameters significantly. ns = $P > 0.05$, * = $P < 0.05$, ** = $P < 0.01$.

901

902 **Figure 10. Cholinergic and NK1 receptor antagonists inhibit Ca^{2+} transients**
903 **elicited by EFS in ICC-DMP.**

904 **A - B** Representative ST maps showing the inhibitory effects of combining
905 cholinergic and neurokinin antagonists (atropine and RP 67580; both 1 μ M) on
906 Ca^{2+} transients in ICC-DMP during EFS (10 Hz; 5 sec). **C – F** Summary data of

907 Ca^{2+} transient parameters showing the inhibitory effects of atropine and RP
908 67580 on Ca^{2+} transient frequency (*C*), amplitude (*D*), duration (*E*) and spatial
909 spread (*F*) in ICC-DMP during the control period, during the final 3 sec of EFS,
910 and during the post-EFS period (5 sec), $n=4$, $c=20$. Note: combination of atropine
911 and RP 67580 abolished all Ca^{2+} transient parameters significantly. $ns = P >$
912 0.05 , $** = P < 0.01$, $*** = P < 0.001$, $**** = P < 0.0001$.

913

914 **Figure 11. Excitatory responses are modestly reduced by atropine**

915 **A - B** Representative ST maps showing the inhibitory effects of atropine ($1 \mu\text{M}$)
916 on responses to EFS (10 Hz; 5 sec; indicated by the red line and dotted white
917 box in ST maps). In this experiment L-NNA ($100 \mu\text{M}$) and the P2Y1 receptor
918 antagonist, MRS 2500 ($1 \mu\text{M}$), were present. **C - F** Summary data showing the
919 effects of a combination of L-NNA ($100 \mu\text{M}$), MRS 2500 ($1 \mu\text{M}$) and atropine (1
920 μM) on Ca^{2+} transient frequency (*C*), amplitude (*D*), duration (*E*) and spatial
921 spread (*F*) in ICC-DMP during the control period, during the final 3 sec of EFS,
922 and during the post-EFS period (5 sec), $n=7$, $c=26$. $ns = P > 0.05$, $** = P < 0.01$,
923 $*** = P < 0.001$.

924

925 **Figure 12. Excitatory responses are strongly attenuated by NK1 antagonist**

926 **A - B** Representative ST maps showing the inhibitory effects of RP 67580 ($1 \mu\text{M}$),
927 in the presence of nitric oxide synthase inhibitor L-NNA ($100 \mu\text{M}$) and purinergic
928 P2Y1 receptor antagonist (MRS 2500; $1 \mu\text{M}$) on Ca^{2+} transients in response to
929 nerve stimulation (EFS at 10 Hz 5 sec; indicated by the red line and dotted white

930 box in ST maps). **C – F** Summary data showing the effects of a combination of L-
931 NNA, MRS 2500 and RP 67580 on Ca^{2+} transient frequency (*C*), amplitude (*D*),
932 duration (*E*) and spatial spread (*F*) in ICC-DMP during the control period, during
933 the final 3 sec of EFS, and during the post-EFS period (5 sec), $n=4$, $c=13$. $ns = P$
934 > 0.05 , $** = P < 0.01$.

935

936 **Figure 13. Excitatory responses to EFS are abolished by atropine and NK1**
937 **receptor antagonist**

938 **A - B** Representative ST maps showing inhibition of Ca^{2+} transients by atropine
939 (1 μM) and RP 67580 (1 μM). These experiments were conducted in the
940 presence of L-NNA (100 μM) in the presence of MRS 2500 (1 μM) during and
941 post nerve stimulation periods (EFS at 10 Hz 5 sec; indicated by the red line and
942 dotted white box in ST maps). **C – F** Summary data showing the effects of a
943 combination of L-NNA, MRS 2500 and atropine and RP 67580 on Ca^{2+} transient
944 frequency (*C*), amplitude (*D*), duration (*E*) and spatial spread (*F*) in ICC-DMP
945 during control conditions, Excitatory periods during EFS (final 3 sec) and in the
946 post EFS period, $n=5$, $c=32$. $ns = P > 0.05$, $** = P < 0.01$, $*** = P < 0.001$.

947

948

949 **Movie 1: ICC-DMP Ca^{2+} transient responses to enteric neuronal stimulation**
950 Movie of intracellular Ca^{2+} transients in ICC-DMP labeled with the genetically
951 encoded Ca^{2+} indicator GCaMP3 in response to electrical field stimulation (EFS
952 10Hz, for 5 sec; real-time playback). The top left FOV shows typical elongated

953 ICC-DMP using a 60x objective (original recordings). Note that Ca^{2+} transients
954 fired in stochastic fashion the blue bit-masked cell. The right window shows Ca^{2+}
955 transient particles thresholded ($\text{SNR} \geq 25$ dB, to facilitate visualization of active
956 signals) after differentiation ($\Delta t = 0.5$ s) and smoothing (Gaussian 1.0sd, box size
957 = $3.3 \mu\text{m}$) as shown in the middle window. Scale bar in top left window is $15 \mu\text{m}$
958 and pertains to all windows.

959 The blue overlay of ICC-DMP in the FOV (blue bit-masked cell) was used to
960 construct an ST map of Ca^{2+} -induced fluorescence intensity across the diameter
961 of the cell, which better displays the firing and propagation of Ca^{2+} transients
962 along the length of the cell in response to EFS (lower panel; EFS duration is
963 indicated with the yellow box). The bottom panel shows active area of Ca^{2+}
964 transients across the FOV (area of active particles). Note the cessation of Ca^{2+}
965 transients in response to EFS and enhanced Ca^{2+} firing during post stimulus
966 period. Scale bar in the lower ST map and bottom active area map is $50 \mu\text{m}$.

967

968

969

970

971

972

973

974

975

976 **Tables**

977 **Table 1:** Summary table of cholinergic and neurokinin receptors primer
978 sequences.

979 Table lists muscarinic (M2, M3) and neurokinin (NK1, NK2) receptor gene
980 transcripts that were measured in this study including their name, primer
981 sequences and gene bank accession numbers.

982

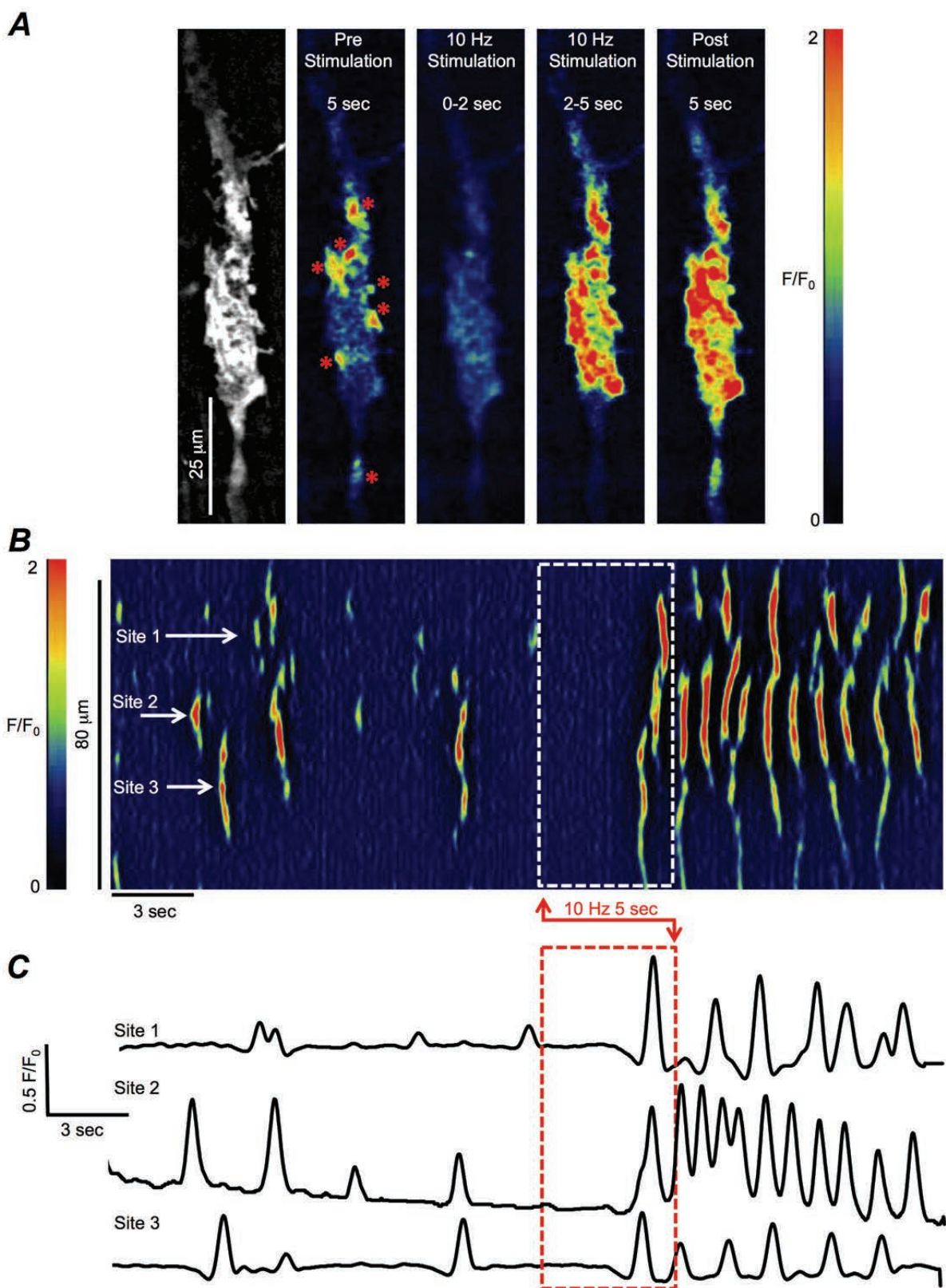
Gene	Sequence	GenBank accession number
<i>mGapdh-F</i>	AGACGGCCGCATCTTCTT	NM_008084
<i>mGapdh-R</i>	TTCACACCGACCTTCACCAT	
<i>mChrm2-F</i>	GGTGTCTCCCAGTCTAGTGCAAGG	NM_203491
<i>mChrm2-R</i>	ATGTCTGCCTAGAGTTGTCATCTTTGGA	
<i>mChrm3-F</i>	TGTGGCCAGCAATGCTTCTGTCATGA	NM_033269
<i>mChrm3-R</i>	CCACAGGACAAAGGAGATGACCCAAG	
<i>mTacr1-F</i>	GTGGTGAACCTTACCTACGCAGTC	NM_009313
<i>mTacr1-R</i>	GCCATGTATGCTTCAAAGGCCACAG	
<i>mTacr2-F</i>	CCATCGCCGCTGACAGGTACA	NM_009314
<i>mTacr2-R</i>	GGCCCCCTGGTCCACAGTGA	

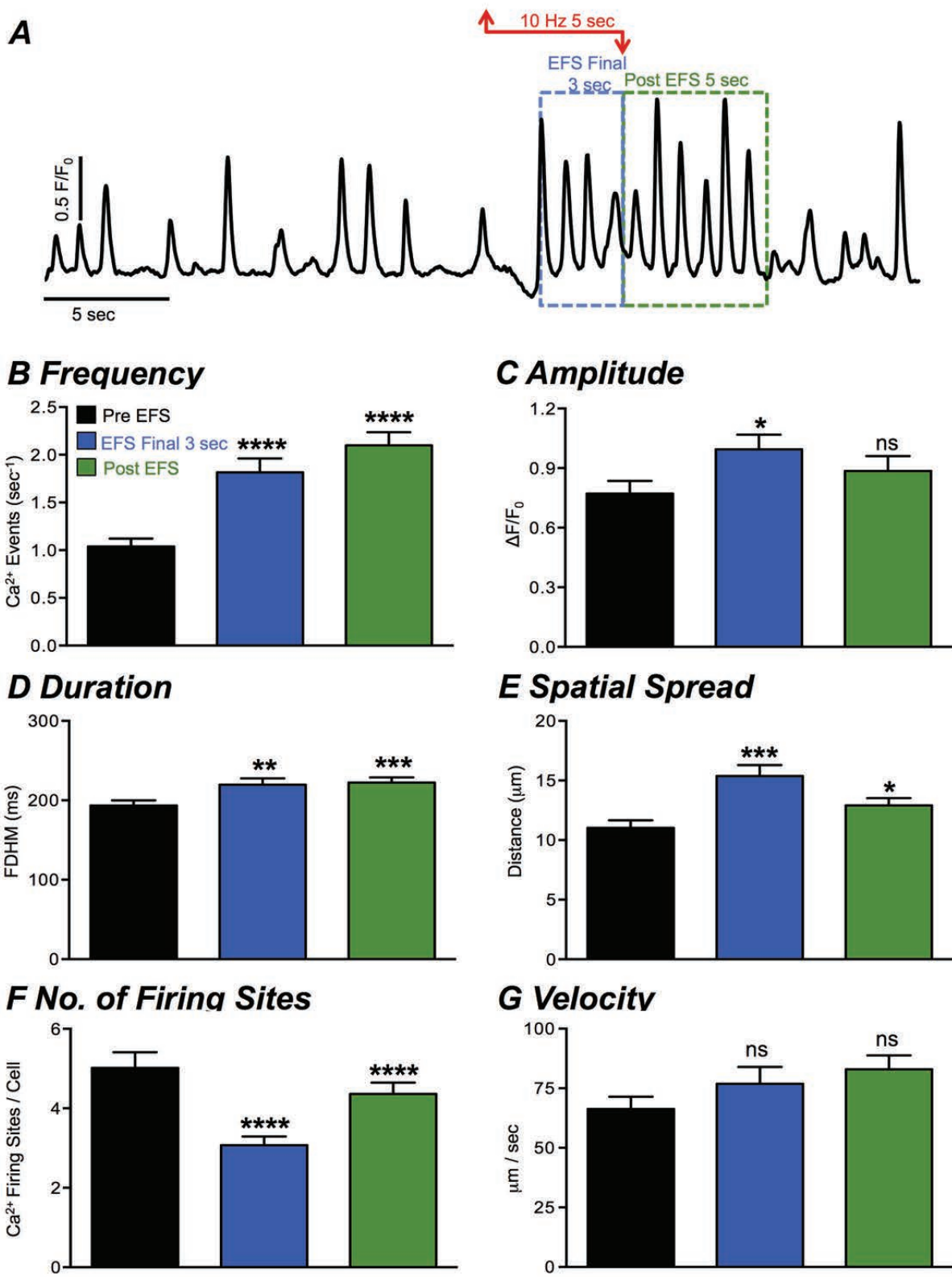
983

984

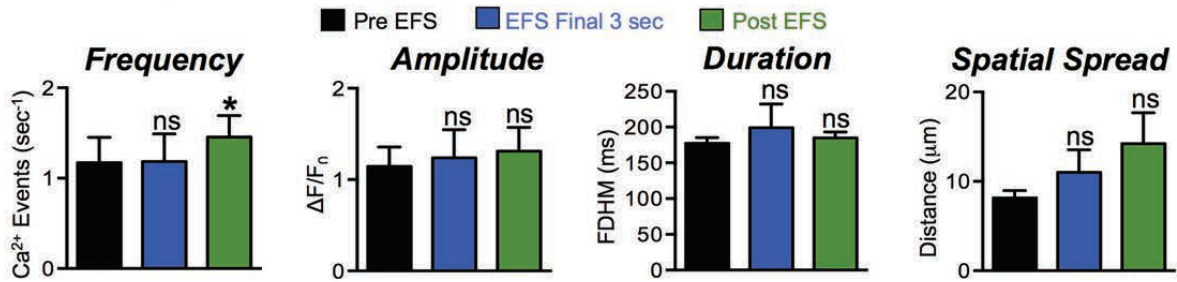
985

986

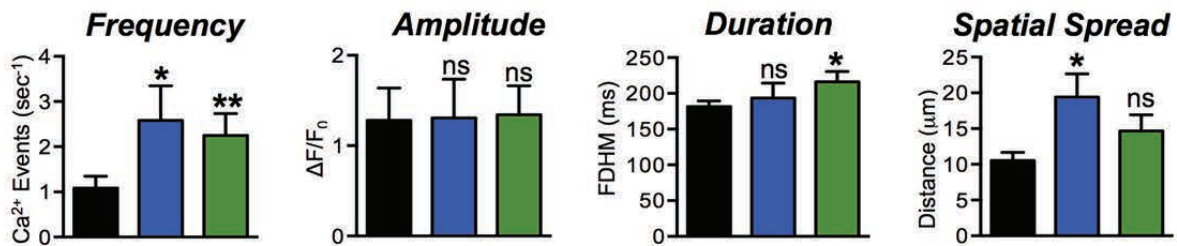




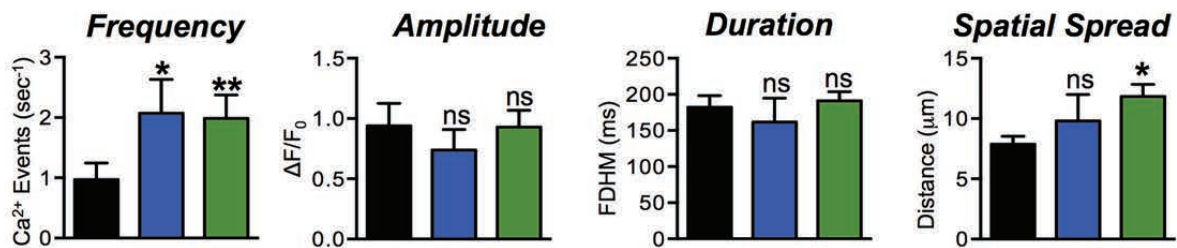
A EFS (1 Hz, 5 Sec)



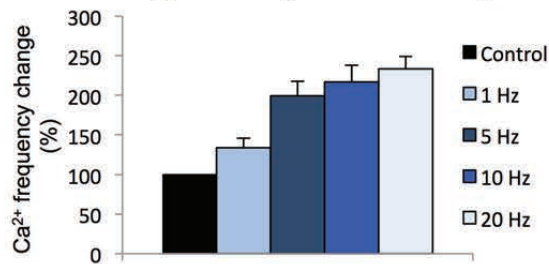
B EFS (5 Hz, 5 Sec)



C EFS (20 Hz, 5 Sec)



D Frequency change during EFS (final 3 sec)



E Frequency change Post stimulus

